LAWRENCE
LIVERMORE
NATIONAL
LABORATORY

UCRL-JRNL-207414

Deliquescence of NaCl-NaNO3, KNO3-NaNO3, and NaCl-KNO3 Salt Mixtures From 90 to 120ºC

S. A. Carroll, L. Craig, T. J. Wolery

October 21, 2004

Geochemical Transactions

Deliquescence of $NaCl$-$NaNO_3$, KNO_3-$NaNO_3$, and $NaCl$-KNO_3 Salt Mixtures From 90 to 120ºC

Susan Carroll[1], Laura Craig, and Thomas J. Wolery

Energy and Environment Directorate, Lawrence Livermore National Laboratory,

Livermore CA 94550

To be submitted to Geochemical Transactions

October 20, 2004

Abstract

We conducted reversed deliquescence experiments in saturated $NaCl$-$NaNO_3$-H_2O, KNO_3-$NaNO_3$-H_2O, and $NaCl$-KNO_3-H_2O systems from 90 to 120ºC as a function of relative humidity and solution composition. $NaCl$, $NaNO_3$, and KNO_3 represent members of dust salt assemblages that are likely to deliquesce and form concentrated brines on high-level radioactive waste package surfaces in a repository environment at Yucca Mountain, NV, USA. Discrepancy between model prediction and experimental code can be as high as 8% for relative humidity and 50% for dissolved ion concentration .

[1] Corresponding Author
Email: carroll6@llnl.gov

The discrepancy is attributed primarily to the use of 25˚C models for Cl-NO_3 and K-NO_3 ion interactions in the current Yucca Mountain Project high-temperature Pitzer model to describe the non-ideal behavior of these highly concentrated solutions.

Key Words

deliquescence, halite, soda niter, niter, brine

1.0 Introduction

Yucca Mountain, Nevada is the designated geologic repository for permanent disposal of high-level nuclear waste. Current waste package design calls for double walled containers with an inner wall of stainless steel and an outer wall of highly corrosion resistant Ni-Cr-Mo alloy, which are protected with Ti shields to prevent rocks and seepage water from contacting the containers (Gordon, 2002). Of concern are the corrosion resistance and long-term integrity of these metal barriers. If the Yucca Mountain site license is approved, the waste packages will be placed in tunnels several hundred meters below the ground surface in partially saturated volcanic tuff, but still well above the groundwater table. A likely source of brines that may potentially corrode metal containers and drip shields are those formed by the absorption of water by hygroscopic salts found in local and regional dust deposited during repository construction and ventilation stages.

Accurate prediction of brine formation is important for the safe disposal of radioactive waste, because brine composition is an indicator of the corrosiveness of the aqueous environment and the relationship between deliquescence relative humidity and temperature is an indicator of "repository dryness". Deliquescence refers to the formation of an aqueous solution by the absorption of water by hygroscopic salt minerals.

This process allows brines to form above 100˚C at standard atmospheric pressure of 1.01325 bar (or above 96˚C and 0.9 bar at the repository elevation of 1039-1107 m; BSC, 2004a, Section 6.7.2.1). The relative humidity at which salts deliquesce is dependent on temperature and is characteristic to each salt mineral or assemblage of salt minerals. For example at 90˚C, $MgCl_2$ deliquesces at 24% relative humidity and KCl deliquesces at 78.5% relative humidity (Greenspan, 1977). Generally, the deliquescence relative humidity for a salt mixture is lower than the deliquescence relative humidity for its pure salt components. Salt deliquescence data are largely limited to 25˚C for mixed salts (Ge et al, 1998; Tang and Munkelwitz, 1993, 1994) and single salts at higher temperatures (Greenspan, 1977).

The range of brines formed by the deliquescence of hygroscopic salts found in dusts can be calculated from mixtures of the pure phases using equilibrium thermodynamics, because relative humidity is related to the activity of water and solution composition. Wolery and Wang (2004) used the EQ3/6 geochemical code and the Yucca Mountain Project high-temperature Pitzer model to predict the deliquescence of salt mixtures found in Yucca Mountain dust samples collected from exploratory tunnels. The modeling results predict that mixtures of NaCl, KNO_3 and/or $NaNO_3$ are the most prevalent mineral assemblages, and that inclusion of KNO_3(s) lowers the deliquescence relative humidity from values near 70% at 25˚C to values as low as 20% at 160˚C. This analysis implies that concentrated brines may contact the metal container and drip shield surfaces at low relative humidity and high temperature.

In this paper we compare model predictions and experimental results of relative humidity and solution compositions for saturated NaCl-$NaNO_3$-H_2O, KNO_3-

$NaNO_3$-H_2O, and NaCl-KNO_3-H_2O systems from 90 to 120ºC. These are benchmark experiments that can be used to assess the validity of the model calculations and Pitzer parameters that account for non-ideal ion interactions in these highly concentrated solutions.

2.0 Model Calculations

Relative humidity is thermodynamically tied to solution composition through the activity of water. The activity of water, a_w, is the product of its mole fraction of water, x_w, and its mole fraction activity coefficient, γ_w:

$$a_w = x_w \gamma_w \qquad 1.$$

The mole fraction of water is dependent on the solution composition:

$$x_w = n_w / (n_w + \sum_i n_i) \qquad 2.$$

where n_w and n_i are the number of moles of water and of dissolved constituent i, respectively. The concentrations of the dissolved constituents are limited by the solubilities of the thermodynamically stable salt minerals. If we use halite (NaCl) as an example, then the solubility product, K_{NaCl}, at a given temperature is dependent on the Na^+ and Cl^- concentrations and activity coefficients according to the mass balance reaction:

$$NaCl(s) = Na^+ + Cl^+ \qquad 3a$$

$$K_{NaCl} = (m_{Na^+} \gamma_{Na^+})(m_{Cl^-} \gamma_{Cl^-}) \qquad 3b$$

where m_i and γ_i indicate the molality and activity coefficient of species *i*, with unit activity implied for the solid (NaCl).

Relative humidity, RH_{frac}, is related to activity of water through the partial pressure of water vapor, and is equivalent to:

$$RH_{frac} = p_w / p_w^o \quad 4.$$

where p_w is the partial pressure of water vapor over an aqueous solution and p_w^o is the partial pressure of water vapor in the standard state over pure water. Similarly, the activity of water is equivalent to:

$$a_w = f_w / f_w^o \quad 5.$$

where f_w is the fugacity of water vapor over an aqueous solution and f_w^o is the fugacity of water vapor in the standard state over pure water. Equating fugacity with its partial pressure:

$$f_w / f_w^o = p_w / p_w^o \quad 6.$$

yields:

$$RH_{frac} = a_w \quad 7.$$

The activity of water is commonly expressed in decimal form and RH is commonly expressed as a percentage; thus $RH\% = 100 \times a_w$.

In hydrologically unsaturated environments, the partial pressure of water cannot exceed the total pressure. The partial pressure of water is related to the vapor pressure of

pure water and the activity of water by $p_w = p_w^o a_w$. Both the vapor pressure of pure water and the partial pressure of water over a salt solution increase strongly with temperature above 100°C. Brines cannot exist at temperatures above the dry-out temperature where the partial pressure of water equals the total pressure. Above the dry-out temperature only solid salt minerals and water vapor occur. Since this process is reversible, the dry-out temperature is also the deliquescence temperature for the same assemblage of salt minerals (note: at much lower temperature, generally 25°C or less, dry-out or "efflorescence" is controlled by salt mineral nucleation instead of equilibrium thermodynamics; Tang and Munkelwitz, 1994). The deliquescence temperature is also equivalent to the boiling point for the saturated solution.

Brines formed by the absorption of water by deliquescent minerals are thermodynamically equivalent to brines that are saturated with respect to the same deliquescent minerals. Figures 1 to 5 show the model calculations of relative humidity and solution composition from 90 to 120ºC versus X_{NO3} or X_{Na} for the NaCl-$NaNO_3$-H_2O, the KNO_3-$NaNO_3$-H_2O, and the NaCl-KNO_3-H_2O systems. For the NaCl-$NaNO_3$-H_2O system, this is done by adding soda niter ($NaNO_3$) to a halite (NaCl) saturated solution until the solution is saturated with both soda niter and halite. This represents the eutectic point for the NaCl-$NaNO_3$ salt assemblage. The calculation for this assemblage is completed by a complementary run in which halite is added to a soda niter saturated solution until the same eutectic point is reached. An identical approach is used for the KNO_3-$NaNO_3$-H_2O and NaCl-KNO_3-H_2O systems. We use the EQ3/6 geochemical code (Wolery and Jarek, 2003) and the Yucca Mountain Project high-temperature Pitzer model (BSC, 2004b). This model is based on the Pitzer equations (cf. Pitzer, 1991) to account

for the non-ideal behavior of the brine solutions. Reaction pressure was allowed to vary by means of the 1.013-bar/steam-saturation curve. The Pitzer model is based on the available experimental data and includes binary interactions ($\beta^{(0)}_{M,X}$, $\beta^{(1)}_{M,X}$, $\beta^{(2)}_{M,X}$, $C^{\phi}_{M,X}$) between two different kinds of ions of opposite charge (cation M and anion X), and also binary ($\theta_{M,M'}$, $\theta_{X,X'}$) interactions between ions of like charge and ternary interactions ($\psi_{M,M',X}$, $\psi_{X,X',M}$) involving three ions in common-cation and common-anion ternary systems. Pitzer parameters relevant to this study are listed in Table 1.

3.0 Experimental Methods

3.1. Starting Materials

Analytical grade sodium chloride (NaCl), sodium nitrate ($NaNO_3$), and potassium nitrate (KNO_3) were used to synthesize dissolved and dry salt mixtures. Distilled and deionized (18 M-ohm) water was used to make all solutions.

3.2. Reverse Deliquescence Experiments

We measured brine composition at controlled relative humidity for NaCl-$NaNO_3$, KNO_3-$NaNO_3$, and NaCl-KNO_3 salt mixtures from 90 to 120˚C as a function of X_{NO3} or X_{Na}. Our experimental design mimics the model calculations in that one salt in the binary system will completely dissolve and the dissolution of the other will be limited by its solubility. We approached the equilibrium brine composition by placing identical mole fractions of dissolved and solid salt mixtures in an environmental chamber (Ecosphere, Despatch) at controlled relative humidity and temperature. Under these conditions the dissolved salt mixture evaporates concentrating the solution and precipitating one of the

two salts, and the solid salt mixture absorbs water dissolving the salts until equilibrium is reached.

For each run, four beakers containing the dissolved salts and four beakers containing the solid salts were placed into the chamber and sequential pairs of initially aqueous and initially solid beakers were sampled over time. Figure 6 shows that steady-state relative humidity and solution composition are achieved with in the first 200 hours of reaction and that solution composition of initially dissolved and initially solid samples converge over the time period of the experiments. Samples were typically taken every one to three days. Calibrated temperature and relative humidity probes were place just above the solutions in the beakers, because microenvironments within the beakers differed from the environmental chamber relative humidity by as much as 5% relative humidity. Relative humidity probe calibration checks were conducted in saturated KNO_3 solutions from 90 to 110˚C. Statistical analysis of these RH measuremements together with vapor pressure measurements for KNO_3 (Kracek, 1928) yield an average standard deviation of about 1.6 RH units. Uncertainty reported in the tables and figures is calculated as 2σ (3.1 this experimentally, because the total pressure in environmental chambers is below the vapor pressure of saturated KNO_3 solutions at 120˚C.

About one gram of solution was collected from each beaker and filtered through a 0.45μ syringe-less filter into a sampling bottle, the bottle was sealed and weighed to determine sample amount, and then diluted with about 250 grams of distilled and deionized water. All dilution factors were determined gravimetrically. Each time a pair of samples was taken, the temperature and relative humidity probes were moved to monitor the next pair of beakers. Solids from the fourth pair of samples were separated

from the remaining solution by filtration (0.45μ pore size), dried, and stored in a desiccator until analyzed by powder X-ray diffraction.

3.3. Analytical Techniques

All aqueous samples were analyzed by inductively coupled plasma-atomic emission spectrometry (ICP-AES) for sodium, and by ion chromatography (IC) for chloride, nitrate, potassium, and (for some samples) sodium. Analytical uncertainty for the ICP-AES and the IC is less than 2%. Solids were analyzed using powder X-ray diffraction (XRD) for detection of halite, sylvite, soda niter, and niter.

3.4. Calculation of Molal Concentrations

Solution compositions were converted from mg/kg-solution to molality (mol/kg-solvent) by subtracting the weight of the dissolved constituents from the sample weight to calculate the weight of solvent water. We assessed the uncertainty of this method by using it to calculate ionic molalities for several synthesized solutions ranging from 5 to 35 molal at 90 to 105˚C, for which independent gravimetric data had been obtained when these solutions were made up. Molality and X_{Na} derived from solution analyses are generally within 4% and 1% of their respective gravimetric values. These results are cconsistent with the uncertainty of the averaged values reported in Tables 1 - 5.

4.0 Results

The deliquescence of NaCl-$NaNO_3$, KNO_3-$NaNO_3$, and NaCl-KNO_3 salt mixtures from 90 to 120ºC are summarized in Tables 1 to 5 and in Figures 1 to 5. Figures 1 and 2

compare the experimental results of the reversed deliquescence experiments with the model calculations for the NaCl-$NaNO_3$-H_2O system at 90 and 110˚C. Equilibrium is shown by the convergence of the measured relative humidity and solution composition for the initially dissolved and initially solid salt mixtures. Although there is good agreement between experiment and model for solutions X_{NO3}<0.5, there are discrepancies for both solution composition and relative humidity for nitrate-rich solutions near the eutectic. The model overpredicts relative humidity by as much as 8% relative humidity and underpredicts the solution composition by as much as 8 molal (or 40%). At 90ºC, the experimental data suggest a deliquescence relative humidity of 56 %RH (X_{NO3}=0.85) compared to the model prediction of 59 %RH (X_{NO3}=0.92). Similarly at 110ºC, the experimental data suggest a deliquescence relative humidity of 52 %RH (X_{NO3}=0.9) compared to the model prediction of 56 %RH (X_{NO3}=0.97).

Although there are discrepancies in the absolute RH and solution composition, both experiment and model exibit similar trends. Relative humidity decreases from a high value near 75% at low X_{NO3} to a minimum near the eutectic point. Above the eutectic point, the relative humidity increases with increasing X_{NO3} as the deliquescence point of pure soda niter is approached. The higher solubility of soda niter generates nitrate concentrations that are substantially higher than the chloride concentrations above X_{NO3} = 0.5. Chloride concentrations decrease with increasing X_{NO3}, because chloride solubility is limited by the increasing sodium concentrations from dissolving soda niter (the common ion effect).

The solids consisted of halite with trace soda niter below the eutectic and of soda niter with trace halite above the eutectic. Trace amounts of soda niter and halite probably

represent residual solution that was trapped in pore spaces during the filtration process when the salts were dried. Halite should be the only solid phase present below the eutectic because the solution is saturated with respect to halite and undersaturated with respect to soda niter. Above the eutectic, soda niter should be the only solid phase present, because the solution is saturated with respect to soda niter and undersaturated with respect to halite. Only at the eutectic, where both minerals are saturated, would one expect to find both halite and soda niter.

Figure 3 compares the experimental results of the reversed deliquescence experiments with the model calculations for the KNO_3-$NaNO_3$-H_2O system at 90˚C. Similar to the NaCl-$NaNO_3$-H_2O system, the convergence between the measured relative humidity and solution composition for initially dissolved and initially solid salt mixtures indicates that equilibrium was achieved. However, there is poor agreement between experiment and model for both the relative humidity and solution composition. Experimental relative humidity values are as much as 8 percentage points higher than those predicted by the model on the niter side of the eutectic (X_{Na}<0.2). Trends in the experimental data indicate that the deliquescence relative humidity is only slightly higher than the model prediction (about 42%), but yields a more KNO_3 rich brine (about X_{Na} 0.5) than predicted by the model.

A large discrepancy between experiment and model is seen in the solution composition. Dissolved potassium, sodium, and nitrate concentrations follow similar trends as the model predictions, but the absolute concentrations are significantly higher. In the most extreme case, solution compositions are roughly twice the model prediction with experimental sodium = 20 molal, potassium = 22 molal, and nitrate = 42 molal. The

high experimental molal concentrations are not an artifact of deriving the values from solution analyses (see section *3.4*). A test of the analytical methodology using highly concentrated solutions showed that analytically and gravimetrically determined values were generally within 4% of each other. The solids consisted of niter with trace soda niter, below the experimental eutectic and of soda niter with trace niter, above the experimental eutectic. Trace amounts of soda niter or niter probably represent residual solution that was trapped in pore spaces during the filtration process when the salts were dried.

Figures 4 and 5 and compare the experimental results of the reversed deliquescence experiments with the model calculations for the NaCl-KNO_3-H_2O system at 90 and 120˚C. Similar to the other salt systems studied here, the convergence between the measured relative humidity and solution composition for initially dissolved and initially solid salt mixtures indicates that equilibrium was achieved. Values for the deliquescence relative humidity are in agreement at both temperatures. This agreement at the eutectic relative humidity appears to be fortuitous, because there is poor agreement between experiment and model for relative humidity and all solution composition. The extent of the mismatch is much greater at 120˚C than at 90˚C. At 90˚C, the greatest mismatch occurs in KNO_3-rich solutions where the model underpredicts relative humidity by as much as five percentage points and underpredicts solution composition by as much as 4 molal (about 30%). In solutions dominated by NaCl (X_{Na}>0.5), there is reasonable agreement between model and experiment. At 120˚C, the mismatch between experiment and model relative humidity is similar to that at 90˚C. However, at this higher temperature, the model significantly underpredicts the solution composition. In the most

extreme case, solution compositions are roughly twice the model prediction with experimental sodium = 10 molal, potassium = 32 molal, chloride = 5 molal, and nitrate = 42 molal. At 120˚C, atmospheric pressure limits the experiments to 50% relative humidity, so we cannot determine if the model adequately predicts relative humidity and solution composition in NaCl-rich solutions.

Analysis of the solids show that sylvite (KCl) is an important solubility control near the experimental eutectic in agreement with the results of model calculations at these temperatures. At 90˚C, niter, sylvite and minor amounts of halite were detected just to the left of the eutectic ($0.28 \leq X_{Na} \leq 0.31$), and halite, sylvite and minor amounts of niter were detected to the right side of the eutectic ($0.35 \leq X_{Na} \leq 0.40$). As is expected, the solids consisted of niter ($X_{Na} \leq 0.25$) and halite ($X_{Na} \geq 0.60$) on their respective limbs of the phase diagram. At 120˚C, solutions were saturated with repect to niter, sylvite, and halite between most of samples between $0.15 \leq X_{Na} \geq 0.30$. One sample at $X_{Na}=0.14$ contained only niter, two samples at $X_{Na}=0.16$ and $X_{Na}=0.30$ contained niter and halite, but no sylvite. Any trace amounts of salt detected probably represent residual solution that was trapped in pore spaces during the filtration process when the salts were dried.

5.0 Discussion

5.1 Na-Cl, Na-NO_3, and K-NO_3 high-temperature Pitzer models

The comparison of model predictions and experimental results of relative humidity and solution compositions for the NaCl-$NaNO_3$-H_2O, KNO_3-$NaNO_3$-H_2O, and the NaCl-KNO_3-H_2O systems from 90ºC to 120ºC indicate that some parameters used in the current high-temperature Pitzer model do not adequately describes brine chemistry

formed by deliquescence of these salt mixtures. Before we discuss the specific data needs to resolve discrepancies between experimental results and model predictions, we review the basic high-temperature Pitzer model used in these simulations (BSC, 2004b).

The Pitzer model is derived by first defining an expression for the excess Gibbs free energy (G^{EX}) of the total solution (Pitzer, 1991, equation 23):

$$\frac{G^{EX}}{RTw_w} = f(I) + \sum_i \sum_j \lambda_{ij}(I) n_i n_j + \sum_i \sum_j \sum_k \mu_{ijk} n_i n_j n_k \qquad 8.$$

where G^{EX} is the difference or "excess" in the Gibbs free energy between a real solution and an ideal solution defined on the molality composition scale, R is the universal gas constant, T is the absolute temperature, w_w is the mass (kg) of solvent water, f is a Debye-Hückel function that depends on the ionic strength ($I = 1/2 \sum_i m_i z_i^2$), λ_{ij} is a second-order interaction coefficient (also a function of I), μ_{ijk} is a third-order interaction coefficient, n denotes the number of moles of a species, and i, j, and k denote solute species. Here m denotes molality and z the charge number. Note that molality is defined as $m_i = n_i / w_w$. Upon substitution of $m_i w_w$ for n_i(and so forth for the j and k cases) in equation 8, the ionic solute activity coefficient (γ_i) and the solvent osmotic coefficient (ϕ) may be calculated as the partial derivatives with respect to the molality of the ionic solute and the mass of water, respectively:

$$\ln \gamma_i = \left[\partial (G^{EX} / w_w RT) / \partial m_i\right]_{n_w} \qquad 9.$$

$$\phi - 1 = -\left(\partial G^{EX} / \partial w_w\right)_{n_i} / RT \sum_i m_i \qquad 10.$$

(Pitzer, 1991, equations 34 and 35). The activity of water is closely related to the osmotic coefficient ($\ln a_w = -\left(\sum_i m_i / \Omega\right)\varphi$, where Ω is the number of moles of water comprising a one kg mass, approximately 55.51).

Substitution of equation 8 into equations 9 and 10 followed by differentiation yields the fundamental Pitzer equations for the solute activity coefficient and the osmotic coefficient (or alternative forms for the activity of water or the activity coefficient of water). See Pitzer (1991) or BSC (2004b) for full details of the applied forms of the Pitzer equations and the corresponding practical interaction coefficients. Values for the practical interaction coefficients are generally obtained by fitting physical property measurements, such as the osmotic coefficient, the vapor pressure of water over salt solutions, or (less commonly) mineral solubilities.

The model requires only two-ion ($\beta^{(0)}_{MX}$, $\beta^{(1)}_{MX}$, $\beta^{(2)}_{MX}$, C^{ϕ}_{MX}, ${}^{S}\theta_{MM'}$ and ${}^{S}\theta_{XX'}$) and three-ion ($\psi_{MM'X}$ and $\psi_{MXX'}$) interaction parameters in the present study of ionic systems. Here M denotes a cation, M^- a different cation, X an anion, and X^- a different anion. The ${}^{S}\theta_{MM'}$, ${}^{S}\theta_{XX'}$, $\psi_{MM'X}$, and $\psi_{MXX'}$ parameters occur only in mixtures of aqueous electroltyes (e.g., MX-M^-X, MX-MX^-, or more complex mixtures). Within the framework of the standard Pitzer model, the values of the mixing parameters are independent of the possible presence of other types of ions in the solution, and once their values have been determined for a particular system, the same values may be used for all other relevant systems (Pitzer 1991).

The high-temperature Pitzer model (BSC, 2004b) employed in the present study uses the following equation to represent the temperature dependence of each of these ion interaction parameters:

$$\chi(T) = a_1 + \frac{a_1}{(T - T_r)} + a_2 \ln(T / T_r) + a_3(T - T_r) + a_4(T^2 - T_r^2) \qquad 11.$$

where χ represents any of the above practical interaction parameters, T_r is the reference temperature (298.15K), and a_1, a_2, a_3, and a_4 are fitted coefficients. A variety of other forms are extant in the literature (e.g. Møller, 1988; Greenberg and Møller, 1989). For the model used here(BSC, 2004b), data taken from other models (see below) were refit as necessary for consistency with the above temperature function. The differences associated with refitting from a different temperature function are negligible within the temperature ranges of the original fits.

Although the high-temperature Pitzer model used in the present study is a fairly comprehensive one accounting for the non-ideal behavior of highly concentrated electrolytes over a wide range of temperature (nominally 0 to 200˚C), there are still significant data needs for common ions. The present model was founded on earlier high-temperature Pitzer models (Møller, 1988; Greenberg and Møller, 1989, and references cited by them), supplemented by parameter data from several other sources (Holmes et al., 1987; Pabalan and Pitzer, 1987; Clegg and Brimblecombe, 1990ab; Thiessen and Simonson, 1990; He and Morse, 1993; Felmy et al. 1994; Clegg et al 1996; Holmes and Mesmer, 1998; Archer, 2000; Oakes et al., 2000). It is also partly based on refitting of parameterizations from the published literature to the most widely used (standard) form of the Pitzer equations (Rard and Wijesinghe, 2003).

The Yucca Mountain Project high-temperature Pitzer model contains robust thermodynamic submodels for the Na-NO_3, Na-Cl, K-Cl, Na-K, and K-Na-Cl ion interactions. The Na-NO_3 model is based on data from –37 to 152˚C (Archer 2000) that was refit for consistency with the standard Pitzer form. Some degradation in fit quality results from this refitting, increasing the deviation in the osmotic coefficient from about 0.01 to about 0.02 (Rard and Wijesinghe, 2003). Similarly, two-ion and three-ion models in the K-Na-Cl system are based on data from 0 to 300˚C (Pitzer et al., 1984; Møller 1988, Holmes et al, 1978; Holmes and Mesmer, 1983) fit using the standard Pitzer form. In contrast, the K-NO_3 and Cl-NO_3 models are based on only 25˚C data (Pitzer 1991) and there are no parameters for the Na-K-NO_3, Na-Cl-NO_3, or K-Cl-NO_3 ion interactions. Our experimental data in the NaCl-$NaNO_3$-H_2O system indicate that temperature dependent parameters for Cl-NO_3 and/or Na-Cl-NO_3 ion interactions are needed to describe the relative humidity and the solution composition near the eutectic where maximum solubilities are approached. The absence of temperature dependent parameters for K-NO_3 ion interactions in the Yucca Mountain Project high-temperature Pitzer model is the primary cause of the poor prediction of the deliquescence of salt mixtures containing KNO_3 at elevated temperatures (Figures 3-5) as well as the measured % relative humidity and solubility of KNO_3 at elevated temperature (Figure 7). Additionally, some of the mismatch in the NaCl-KNO_3-H_2O may also be due to the absence of temperature dependent paramaters for Cl-NO_3, Na-Cl-NO_3, and/or K-Cl-NO_3 ion interactions, in addition to the absence of temperature dependent K-NO_3 ion interaction parameters.

5.2 Implications for radioactive waste disposal

It is important that geochemical calculations of the chemical environment at the waste package surfaces use a robust high-temperature Pitzer ion interaction model for common ions, because the deliquescence of aerosol salts and dust is likely to be a primary source of brines that contact the waste containers and drip shields. In addition to the discrepancy identified for relative humidity and solution composition for salt mixtures containing KNO_3 stemming from the use of a constant temperature model for K - NO_3 interactions, discrepancies for magnesium and ammonium salt mixtures at elevated temperatures are likely because the model includes constant temperature models for many of their respective ion interactions (BSC 2004b). Osmotic and activity coefficients must be experimentally determined as a function of temperature to derive the ion interaction parameters needed to describe the non-ideal behavior of these concentrated solutions, because the Pitzer model is empirically based. Of the salt systems listed above, robust models for potassium salts are probably the most important at high temperature, because magnesium concentrations are likely to be limited by insoluble silicate minerals (Alai et al., 2004) and ammonium concentrations are likely to be limited by gas volatility.

Recent modeling efforts by the Yucca Mountain Project predict that mixtures of NaCl, KNO_3 and/or $NaNO_3$ are the most prevalent mineral assemblages that may deliquesce in repository environments using the current high-temperature Pitzer model (BSC 2004b). As the temperature increases, the deliquescence relative humidity and the NO_3 concentrations increase (Figure 7). We expect only small differences between predicted and actual deliquescence relative humidity and brine composition at temperatures below 60˚C, because the model adequately predicts niter solubility at these temperatures. However, at higher temperatures, much larger differences between

predicted and actual environment are expected, because the model underpredicts niter solubility by about 200% at 135˚C (Figure 7b). At these temperatures the current Pitzer model will significantly under predict brine NO_3 brine composition because the K-NO_3 interactions will be more important. This is clearly illustrated in our KNO_3-$NaNO_3$ and NaCl-KNO_3 deliquescence experiments, where NO_3 concentrations can be twice the predicted concentrations. Additionally, it is likely that calculated deliquescence relative humidities for the three salt system are of limited accuracy, because the current model for KNO_3 is of limited accuracy at high temperature (Figure 8). Therefore calculated dry-out or deliquescence temperatures are uncertain. Dry-out or deliquescence temperatures made assuming a total pressure similar to current atmospheric pressure (0.90 bar) predict that a brine saturated with NaCl, $NaNO_3$, and KNO_3 would boil just above 135^{o}C (BSC 2004a).

6.0 Conclusions

Adsorption of water by deliquescent salt minerals found in aerosols and dusts that may be deposited on waste package surfaces during the construction and ventilation stages of a high-level radioactive waste repository at Yucca Mountain, NV, USA will be a primary source of brines that might lead to corrosion of the waste package surfaces. Although the deliquescence relative humidity of most pure salt minerals is known over a range of temperature, the behavior of salt mixtures at elevated temperatures is unknown. Our reversed deliquescent experimental results in saturated NaCl-$NaNO_3$-H_2O, KNO_3-$NaNO_3$-H_2O, and NaCl-KNO_3-H_2O systems from 90 to 120ºC show that use of 25ºC parameter values for K-NO_3 and Cl-NO_3 (and possibly for three-ion parameters in the

Na-K-Cl-NO_3 system) in the Yucca Mountain Project high-temperature Pitzer model do not accurately predict the equilibrium solubility and corresponding relative humidity of KNO_3 salt mixtures and of NaCl-$NaNO_3$ mixtures near the eutectic composition.

Acknowledgements

This work was performed under the auspices of the U. S. Department of Energy by the University of California, Lawrence Livermore National Laboratory under Contract No. W-7405-Eng-48.

References

Alai, M., Sutton, M., and Carroll, S. 2004. Evaporation evolution of brines from synthetic Topopah Spring Tuff pore water, Yucca Mountain, USA, submitted to Geochemical Transactions.

Archer,D. G., 2000. Thermodynamic properties of the $NaNO_3 + H_2O$ System. J. Phys Chem. Ref. Data, 29: 1141-1156.

BSC (Bechtel SAIC Company), 2004a. Environment on the Surfaces of the Drip Shield and Waste Package Outer Barrier. ANL-EBS-MD-000001 REV 01. Las Vegas, Nevada.

BSC (Bechtel SAIC Company), 2004b. In-Drift Precipitates/Salts Model. ANL-EBS-MD-000045 REV 02. Las Vegas, Nevada: Bechtel SAIC Company.

Clegg, S. L. and Brimblecombe, P., 1990a. Equilibrium partial pressures and mean activity and osmotic coefficients of 0-100% nitric acid as a function of temperature. J. Phys. Chem., 94: 5369-5380.

Clegg, S. L. and Brimblecombe, P., 1990b. The solubility and activity coefficient of oxygen in salt solutions. Geochimica Cosmochimica Acta, 54: 3315-3328.

Clegg, S. L., Milioto, S., and Palmer, D. A., 1996. Osmotic and activity coefficients of aqueous $(NH_4)_2SO_4$ as a function of temperature and $(NH_4)_2SO_4$-H_2SO_4 mixtures at 298.15 K and 323.15 K. J. Chem. Eng. Data, 41: 455-467.

Felmy, A. R., Schroeder, C. C. and Mason, M. J., 1994. A solubility model for amorphous silica in concentrated electrolytes, PNL-SA-25345, Pacific Northwest National laboratory, Richland, Washington.

Ge, Z., Wexler, A.S., and Johnston, M.V., 1998. Deliquescence behavior of multicomponent aerosols. Journal of Physical Chemistry A, 102: 173-180

Gordon, G. M., 2002. Corrosion considerations related to permanent disposal of high-level radioactive waste. J. Sci. Eng. Corrosion, 58: 811-825.

Greenberg, J. P. and Møller, N., 1989. The prediction of mineral solubilities in natural waters: A chemical equilibrium model for the Na-K-Ca-Cl-SO_4-H_2O system to high concentration from 0 to 250 °C. Geochim. Cosmochim. Acta, 53: 2503–2518.

Greenspan, L., 1977. Humidity fixed points of binary saturated aqueous solutions. Journal of Research of the National Bureau of Standards, 81A: 89-96.

He, S. and Morse, J. W., 1993. The carbonic acid system and calcite solubility in aqueous Na-K-Ca-Mg-Cl-SO_4 solutions from 0 to 90˚C. Geochim. Cosmochim. Acta, 57: 3533-3554.

Holmes, H. F., Busey, R. H. Simonson, J. M, and Mesmer, R. E., 1987. The Enthalpy of dilution of HCl(aq) to 648 K and 40 MPa.. J. Chem. Thermodynamics, 19: 863-890.

Holmes, H. F. and Mesmer, R. E., 1998. An isopiestic study of aqueous solutions of the alkali metal bromides at elevated temperatures. J. Chem. Thermodynamics, 30: 723-741.

Kracek, F. C., 1928. P-T-X relations for systems of two or more components and containing two or more phases (L-V), (L_I,L_{II}-V and S-L-V systems), International Critical Tables of Numerical Data, Physics, Chemistry and Technology (ed. E. Washburn) 3: 351-374.

Linke, W. F. 1965. Solubilities: Inorganic and Metal-Organic Compounds. V. 2, K-Z. 4th Edition, Washington, D. C., American Chemical Society, 250p.

Møller, N., 1988. The prediction of mineral solubilities in natural waters: A chemical equilibrium model for the Na-Ca-Cl-SO_4-H_2O system to high temperature and concentration. Geochim. Cosmochim. Acta, 52: 821-837.

Oakes, C. S., Felmy, A. R., and Sterner, S. M., 2000. Thermodynamic properties of aqueous calcium nitrate {$Ca(NO_3)_2$} to the temperature 373 K including new enthalpy of dilution data. J. Chem. Thermodynamics, 32: 29-54.

Pabalan, R. T. and Pitzer, K. S., 1987. Thermodynamics of concentrated electrolyte mixtures and the prediction of mineral solubilities to high temperatures for mixtures in the system Na-K-Mg-Cl-SO_4-OH-H_2O. Geochimica Cosmochimica Acta, 51: 2429-2443.

Pitzer, K. S., Peiper, J. C., and Busey, R. H., 1984. Thermodynamic properties of aqueous sodium chloride solutions. J. Phys. Chem. Ref. Data, 13: 1-102.

Pitzer, K. S., 1991. Ion interaction approach: Theory and data correlation. In: K. S. Pitzer, (Editor) Activity Coefficients in Electrolyte Solutions, 2nd. Ed, CRC Press: Boca Raton, FL, pp. 75–153.

Rard, J. A. and Wijesinghe, A. M., 2003. Conversion of parameters between different variants of Pitzer's ion-interaction model, both with and without ionic strength dependent higher-order terms. J. Chemical Thermodynamics, 35: 439–473.

Tang, I.N., and Munkelwitz, H.R., 1993. Composition and temperature dependence of the deliquescence properties of hygroscopic aerosols. Atmospheric Environment, 27A: 467-473.

Tang, I.N., and Munkelwitz, H.R., 1994. Aerosol phase transformation and growth in the atmosphere. Journal of Applied Meteorology, 33: 791-796.

Thiessen, W. E. and Simonson, J. M., 1990. Enthalpy of dilution and the thermodynamics of NH4Cl(aq) to 523 K and 35 MPa. J. Phys. Chem., 94: 7794-7800.

Wolery, T. J. and Jarek, R. L., 2003. EQ3/6, Version 8.0, Software User's Manual, Software Document Number: 10813-UM-8.0-00, U.S. Department of Energy, Office of Civilian Radioactive Waste Management, Office of Repository Development, 1261 Town Center Drive, Las Vegas, Nevada 89144.

Wolery, T. and Wang, Y. 2004. Deliquescence of salts: Concept of key mineral assemblages. *In* Water-Rock Interaction, Wanty and Seal II, editors., V.2, p.1023-1026.

Table 1. Pitzer interaction parameters used with EQ3/6 to calculate relative humidity and solution composition in saturated brines containing Na, K, Cl and NO_3.

	Pitzer Interaction Parameters					
Ion Interactions	**Coefficients**	**a_1**	**a_2**	**a_3**	**a_4**	**Reference**
K - Cl	$\beta^{(0)}_{MX}$	4.78×10^{-02}	$-3.43 \times 10^{+02}$	-1.38	1.34×10^{-03}	Greenberg and Moller, 1989
	$\beta^{(1)}_{MX}$	2.16×10^{-01}	$-5.76 \times 10^{+02}$	-2.88	4.64×10^{-03}	
	$\beta^{(2)}_{MX}$	0.00				
	C^{ϕ}_{MX}	-7.49×10^{-04}	$3.65 \times 10^{+01}$	1.48×10^{-01}	-1.47×10^{-04}	
K - NO_3	$\beta^{(0)}_{MX}$	-8.16×10^{-02}				Pitzer, 1991
	$\beta^{(1)}_{MX}$	4.94×10^{-02}				
	$\beta^{(2)}_{MX}$	0.00				
	C^{ϕ}_{MX}	6.60×10^{-03}				
Na - Cl	$\beta^{(0)}_{MX}$	7.46×10^{-02}	$-4.71 \times 10^{+02}$	-1.85	1.66×10^{-03}	Greenberg and Moller, 1989
	$\beta^{(1)}_{MX}$	2.75×10^{-01}	$-5.21 \times 10^{+02}$	-2.88	4.71×10^{-03}	
	$\beta^{(2)}_{MX}$	0.00				
	C^{ϕ}_{MX}	1.54×10^{-03}	$4.81 \times 10^{+01}$	1.75×10^{-01}	-1.56×10^{-04}	
Na - NO_3	$\beta^{(0)}_{MX}$	3.57×10^{-03}	$-7.03 \times 10^{+02}$	-3.35	3.98×10^{-03}	Archer, 2000
	$\beta^{(1)}_{MX}$	2.32×10^{-01}	$-2.73 \times 10^{+03}$	$-1.30 \times 10^{+01}$	2.07×10^{-02}	
	$\beta^{(2)}_{MX}$	0.00				
	C^{ϕ}_{MX}	-4.15×10^{-05}	$6.48 \times 10^{+01}$	3.18×10^{-01}	-3.84×10^{-04}	
K-Na	${}^{S}\theta_{MM'}$	-3.20×10^{-03}	$1.40 \times 10^{+01}$	9.09×10^{-13}	-2.66×10^{-15}	Greenberg and Moller, 1989
Cl - NO_3	${}^{S}\theta_{XX'}$	1.60×10^{-02}				Pitzer, 1991
K - Na - Cl	$\psi_{MM'X}$	-3.69×10^{-03}	-5.10	-3.41×10^{-13}	6.66×10^{-16}	Greenberg and Moller, 1989

Table 2. Solution %RH and composition from reversed deliquescence of NaCl-$NaNO_3$ mixtures at 90ºC. Reported values represent the average steady-state solution composition.

Exper. ID	T ˚C	%RH ±3.1	Na molal	Cl molal	NO_3 molal	$[NO_3]/[NO_3]+[Cl]$
Initially Dissolved Salt						
MS-9A	91	74.6	7.44±0.01	6.60±0.03	0.85±0.00	0.11±0.00
MS-10A	90	69.3	9.70±0.16	5.29±0.01	4.50±0.02	0.46±0.00
MS-11A	90	57.6	19.09±0.09	1.83±0.00	17.30±0.01	0.91±0.00
MS-12A	90	59.6	16.74±0.98	3.56±0.27	13.31±0.62	0.79±0.00
MS-13A	90	55.8	18.14±0.41	2.79±0.10	15.10±0.13	0.84±0.00
Initially Solid Salt						
MS-9B	91	74.7	7.74±0.02	6.48±0.00	1.27±0.00	0.16±0.00
MS-10B	91	69.2	9.75±0.25	4.86±0.10	4.86±0.12	0.50±0.00
MS-11B	91	57.6	19.20±0.06	1.87±0.00	17.68±0.08	0.90±0.02
MS-12B	91	59.4	16.59±0.12	3.39±0.08	13.54±0.08	0.80±0.01
MS-13B	91	55.7	18.70±0.48	2.84±0.03	15.73±0.18	0.85±0.00

Table 3. Solution %RH and composition from reversed deliquescence of NaCl-$NaNO_3$ mixtures at 110ºC. Reported values represent the average steady-state solution composition.

Exper. ID	T ˚C	%RH ±3.1	Na molal	Cl molal	NO_3 molal	$[NO_3]/[NO_3]+[Cl]$
Initially Dissolved Salt						
MS45-A	110	52.3	23.25±0.44	2.34±0.00	20.75±0.06	0.90±0.01
MS46-A	110	56.3	19.23±0.20	3.17±0.01	16.01±0.25	0.83±0.00
MS47-A	110	60.3	15.96±0.20	3.63±0.01	12.64±0.15	0.78±0.00
MS48-3A	110	69.6	9.53±0.01	5.62±0.00	4.07±0.02	0.42±0.02
MS49-4A	110	65.6	12.54±0.02	4.65±0.01	7.97±0.03	0.63±0.01
MS50R-A	110	54.9	22.02±0.55	0.43±0.01	21.26±0.58	0.98±0.01
Initially Solid Salt						
MS45B	110	51.5	22.84±0.03	2.53±0.00	20.56±0.03	0.89±0.01
MS46-B	110	55.8	19.77±0.30	3.06±0.01	16.57±0.25	0.84±0.00
MS47-B	110	59.6	16.48±0.27	3.42±0.08	13.30±0.18	0.80±0.00
MS48-3B	110	69.0	9.99±0.00	5.25±0.01	4.79±0.01	0.48±0.01
MS49-4B	110	64.8	13.62±0.03	4.07±0.01	9.65±0.00	0.70±0.01
MS50R-B3	110	54.5	22.34±0.02	0.87±0.00	21.37±0.01	0.96±0.00

Table 4. Solution % RH and composition from reversed deliquescence of $NaNO_3$-KNO_3 mixtures at 90ºC. Reported values represent the average steady-state solution composition, unless otherwise noted.

Exper. ID	T ˚C	%RH ±3.1	Na molal	K molal	NO_3 molal	[Na]/ [Na]+[K]
Initially Dissolved Salt						
MS-14A1	90	65.5	3.35±0.01	18.15±0.04	22.02±0.076	0.16±0.00
MS-14A	90	67.5	1.44±0.39	18.27±0.13	20.40±0.12	0.07±0.02
MS-15A	90	58.6	18.81±0.10	1.01±0.04	20.23±0.64	0.95±0.00
MS-16A	90	55.5	20.36±0.95	2.54±0.26	23.02±0.90	0.89±0.01
MS-17A	90	55.6	10.77±0.59	19.67±1.47	31.04±2.52	0.35±0.01
MS-18A	90	50.3	14.84±0.41	20.16±0.36	35.47±0.86	0.42±0.00
MS-19A	90	50.6	21.40±0.26	9.00±0.50	30.89±0.80	0.70±0.01
MS-20A	90	45.0	18.67±0.27	21.65±0.72	40.24±0.68	0.46±0.01
MS-21A	90	45.6	22.82±0.98	16.43±0.42	39.17±1.36	0.58±0.01
Initially Solid Salt						
MS-14B	90	67.4	2.36±0.17	17.93±0.63	20.82±0.63	0.116±0.00
MS-15B	90	58.3	18.53±0.79	1.12±0.23	20.47±1.32	0.943±0.01
MS-16B	90	55.2	20.32±0.98	3.33±0.30	23.36±0.73	0.860±0.01
MS-17B3	90	55.3	10.94±0.00	18.58±0.33	30.01±0.03	0.371±0.01
MS-18B3	90	50.4	14.44±0.05	19.72±0.05	33.66±0.02	0.423±0.01
MS-19B	90	50.7	21.66±0.60	9.80±0.90	31.84±0.66	0.689±0.02
MS-20B	90	45.5	19.71±0.46	22.53±0.40	42.48±0.71	0.467±0.01
MS-21B	90	45.9	22.54±0.58	16.37±0.15	38.95±0.94	0.579±0.01

Table 5. Solution %RH and composition from reversed deliquescence of NaCl-KNO_3 mixtures at 90ºC. Reported values represent the average steady-state solution composition.

Exper. ID	T ˚C	%RH ±3.1	Na molal	K molal	Cl molal	NO_3 molal	[Na]/ [Na]+[K]
Initially Dissolved Salt							
MS-24A3	90	62.4	2.68±0.00	16.29±0.02	2.54±0.00	16.84±0.01	0.14±0.00
MS-25A4	90		6.07±0.01	6.56±0.04	5.82±0.01	6.58±0.01	0.48±0.01
MS-26A	90	55.3	4.75±0.14	15.36±0.20	4.71±0.08	15.95±0.30	0.24±0.01
MS-27A	90	54.7	7.07±0.34	11.97±1.04	5.80±0.08	13.64±1.49	0.37±0.01
MS-28A	90	65.5	1.55±0.11	18.09±0.04	1.63±0.06	18.07±0.05	0.08±0.01
MS-29A	90	65.3	5.71±0.09	3.71±0.23	5.79±0.05	3.74±0.22	0.61±0.01
MS-30A	90	71.5	5.43±0.00	0.42±0.07	5.53±0.01	0.44±0.06	0.93±0.01
MS-31A	90	52.4	5.96±0.25	15.85±0.39	5.06±0.09	16.74±0.40	0.27±0.00
MS-32A4	90	52.4	7.17±0.02	12.48±0.07	5.51±0.02	14.46±0.00	0.36±0.01
MS-35A4	90	56.4	6.61±0.07	9.90±0.03	5.93±0.00	10.29±0.05	0.40±0.01
MS-36A	90	51.5	6.98±0.43	16.68±0.38	5.35±0.06	17.91±0.05	0.29±0.02
MS-37A	90	50.7	8.00±0.06	14.91±0.07	5.56±0.04	17.59±0.12	0.35±0.00
Initially Solid Salt							
MS-24B3	90	62.5	2.72±0.02	16.96±0.04	2.82±0.00	17.29±0.02	0.14±0.00
MS-25B4	90	62.8	6.22±0.01	6.61±0.06	5.89±0.04	6.68±0.01	0.48±0.01
MS-26B	90	55.6	4.99±0.05	15.40±0.37	4.93±0.04	16.08±0.22	0.24±0.00
MS-27B	90	55.7	7.17±0.40	12.48±1.45	5.73±0.09	14.11±1.91	0.37±0.01
MS-28B	90	65.7	1.64±0.09	18.10±0.20	1.82±0.09	18.08±0.21	0.08±0.00
MS-29B	90	65.6	5.81±0.02	4.09±0.21	5.80±0.01	4.08±0.23	0.59±0.01
MS-30B	90	71.9	5.54±0.02	1.03±0.04	5.60±0.02	1.05±0.03	0.84±0.00
MS-31B	90	52.7	6.57±0.16	16.04±0.04	5.34±0.11	17.28±0.07	0.29±0.00
MS-32B4	90	52.8	7.47±0.02	13.08±0.08	5.43±0.01	15.33±0.01	0.36±0.00
MS-35B4	90	55.8	6.91±0.06	10.57±0.07	5.60±0.02	11.54±0.02	0.40±0.01
MS-36B	90	50.9	7.53±0.20	16.50±0.22	5.52±0.11	18.18±0.28	0.31±0.00
MS-37B	90	51.1	8.06±0.07	15.12±0.11	5.58±0.05	17.70±0.18	0.35±0.00

Table 6. Solution %RH and composition from reversed deliquescence of NaCl-KNO_3 mixtures at 120ºC. Reported values represent the average steady-state solution composition.

Exper. ID	T ˚C	%RH ±3.1	Na molal	K molal	Cl molal	NO_3 molal	Na]/ [Na]+[K]
Initially Dissolved Salt							
MS-34A(44)	120	43.0	8.35±0.00	17.19±0.32	6.14±0.00	20.22±0.05	0.33±0.01
MS-34A(41)	120	41.6	10.98±0.03	27.72±0.06	5.95±0.00	33.43±0.14	0.28±0.01
MS-34A(48	120	48.1	8.18±0.06	16.55±0.25	6.09±0.02	19.27±0.06	0.33±0.01
MS-39A	119	47.3	9.14±0.07	20.33±0.13	6.09±0.04	23.85±0.09	0.31±0.01
MS-40A	119	47.9	5.54±0.05	30.26±0.08	5.53±0.00	30.38±0.13	0.16±0.00
MS-41A	119	45.7	9.86±0.05	22.09±0.03	6.22±0.02	26.44±0.06	0.31±0.01
MS-42A2	119	43.8	7.35±0.02	30.14±0.14	5.60±0.00	31.62±0.03	0.20±0.00
MS-43A2	119	43.3	10.65±0.03	24.90±0.04	6.00±0.03	29.29±0.17	0.30±0.00
MS-44A(40)	119	41.9	8.57±0.01	29.30±0.18	5.71±0.00	32.51±0.03	0.23±0.00
MS-44A(41)	119	42.9	8.19±0.01	29.28±0.09	5.45±0.00	31.94±0.05	0.22±0.00
Initially Solid Salt							
MS-33B(48)	120	48.7	4.64±0.03	27.60±0.22	4.60±0.03	27.94±0.03	0.14±0.00
MS-34B(44)	120	45.3	9.45±0.09	26.16±0.16	5.74±0.00	30.67±0.07	0.27±0.01
MS-34B(41)	120	41.0	10.89±0.03	28.53±0.11	5.92±0.00	34.26±0.06	0.28±0.01
MS-34B(48)	119	49.0	8.11±0.02	18.20±0.27	5.76±0.02	21.47±0.03	0.31±0.01
MS-38B	119	46.9	5.30±0.01	28.48±0.16	5.31±0.02	28.50±0.03	0.16±0.00
MS-39B	120	46.9	10.11±0.02	23.21±0.01	6.15±0.03	28.05±0.00	0.30±0.01
MS-40B	119	46.2	5.84±0.01	31.11±0.01	5.86±0.00	31.62±0.16	0.16±0.00
MS-41B	119	46.1	10.02±0.03	23.20±0.06	6.01±0.02	27.25±0.15	0.30±0.00
MS-42B2	119		7.37±0.01	31.58±0.16	5.83±0.00	33.11±0.01	0.19±0.00
MS-43B2	120	43.6	11.24±0.01	26.87±0.05	6.36±0.01	31.73±0.08	0.30±0.00
MS-44B(40)	119	41.3	9.11±0.05	28.91±0.31	5.69±0.01	32.42±0.02	0.24±0.00
MS-44B(41)	119	42.4	8.37±0.03	29.79±0.51	5.72±0.01	32.65±0.10	0.22±0.00

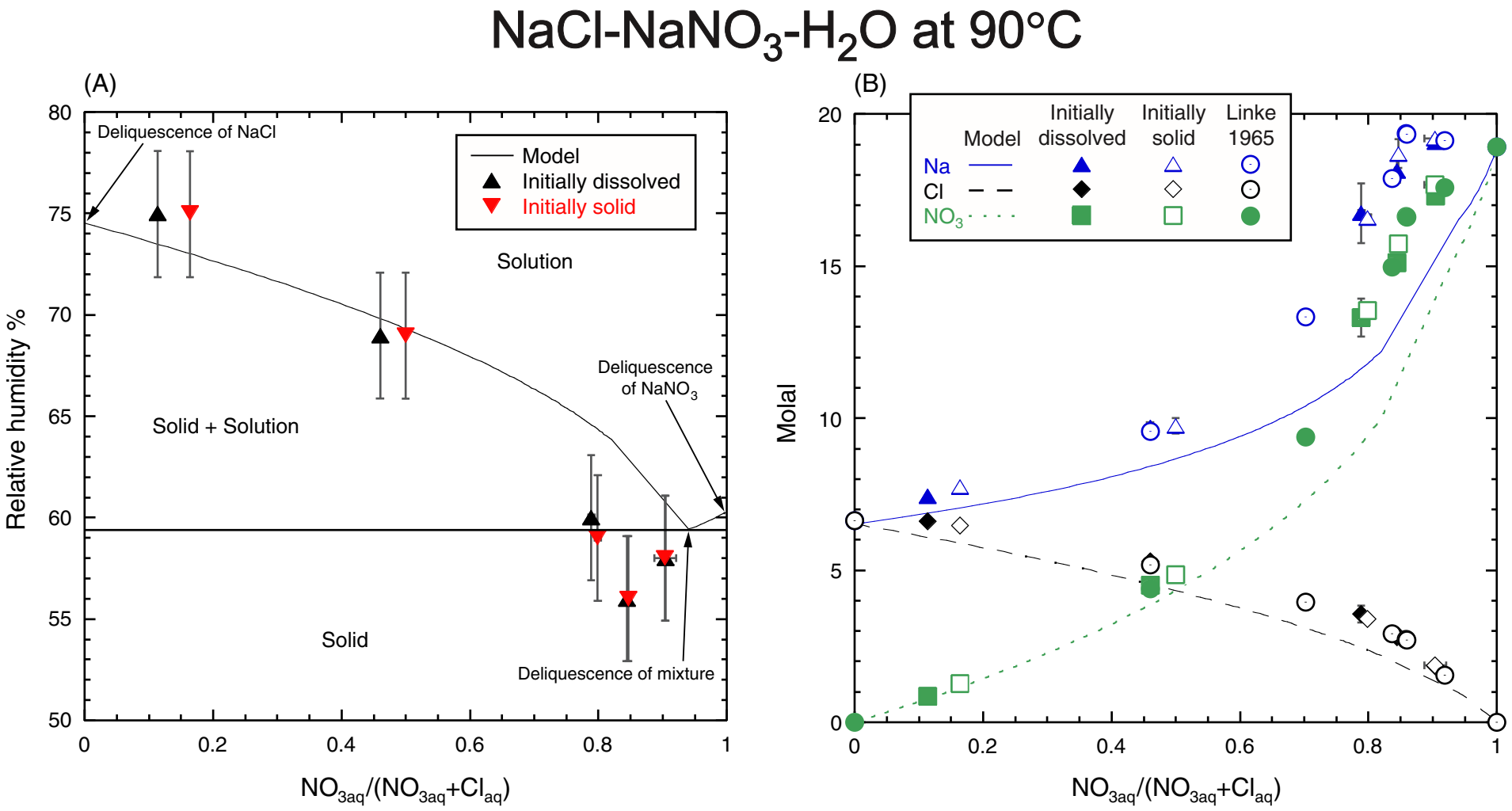

Figure 1. Deliquescence of NaCl-$NaNO_3$ salts at 90ºC starting from initially dissolved and initially solid mixtures plotted as (A) % relative humidity and (B) solution composition.

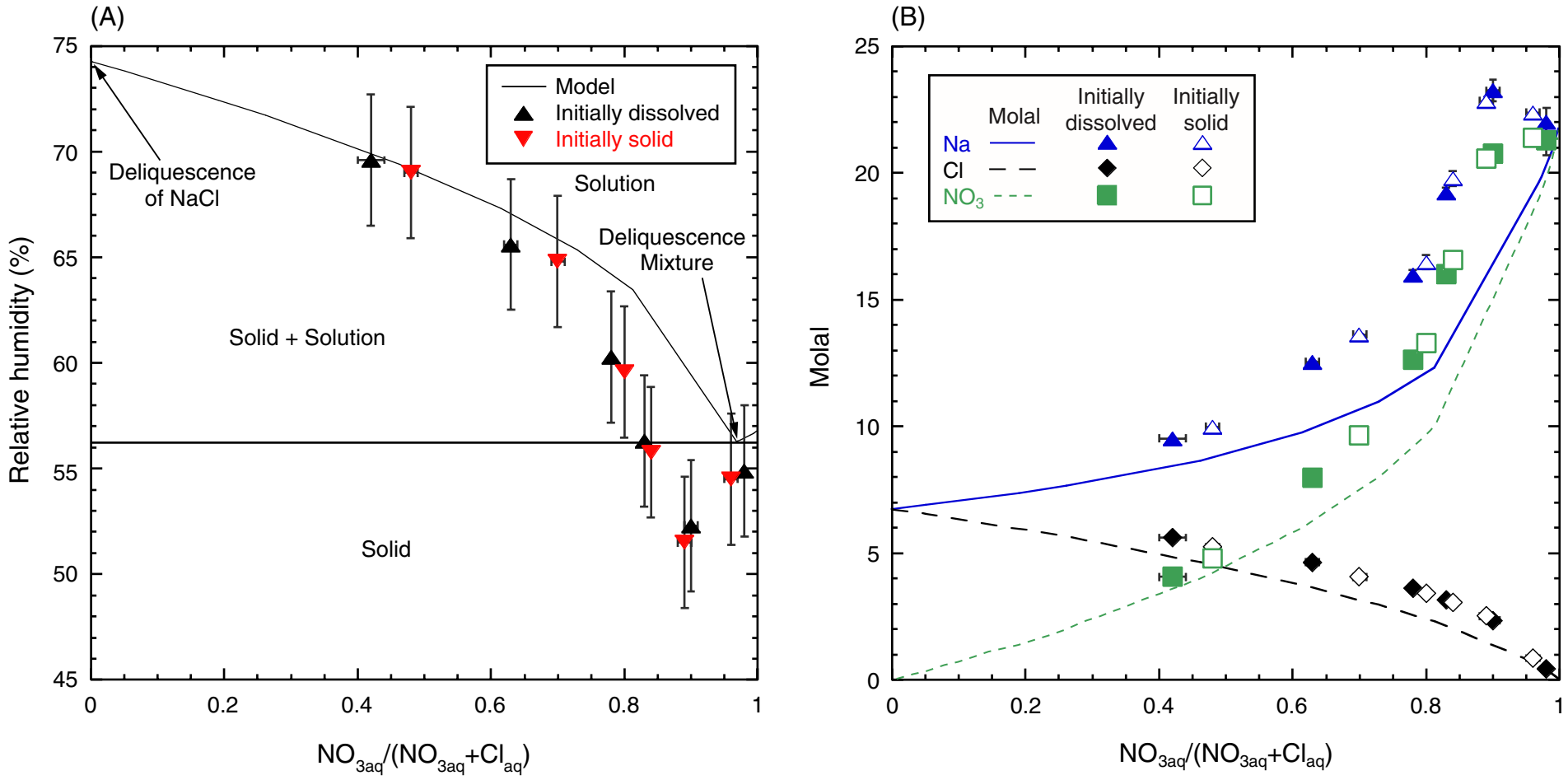

Figure 2. Deliquescence of NaCl-$NaNO_3$ salts at 110ºC starting from initially dissolved and initially solid mixtures plotted as (A) % relative humidity and (B) solution composition.

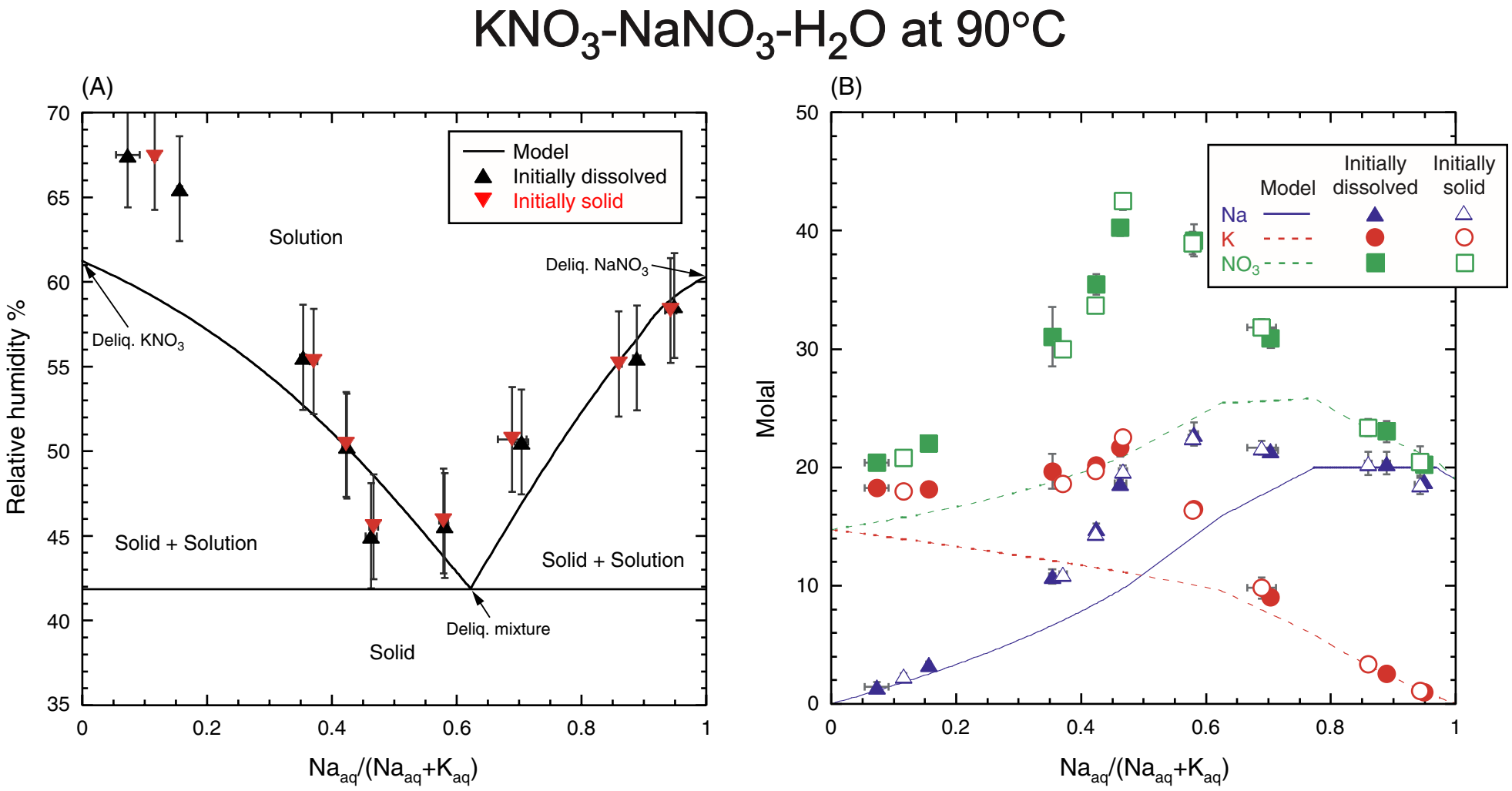

Figure 3. Deliquescence of $NaNO_3$-KNO_3 salts at 90ºC starting from initially dissolved and initially solid mixtures plotted as (A) % relative humidity and (B) solution composition.

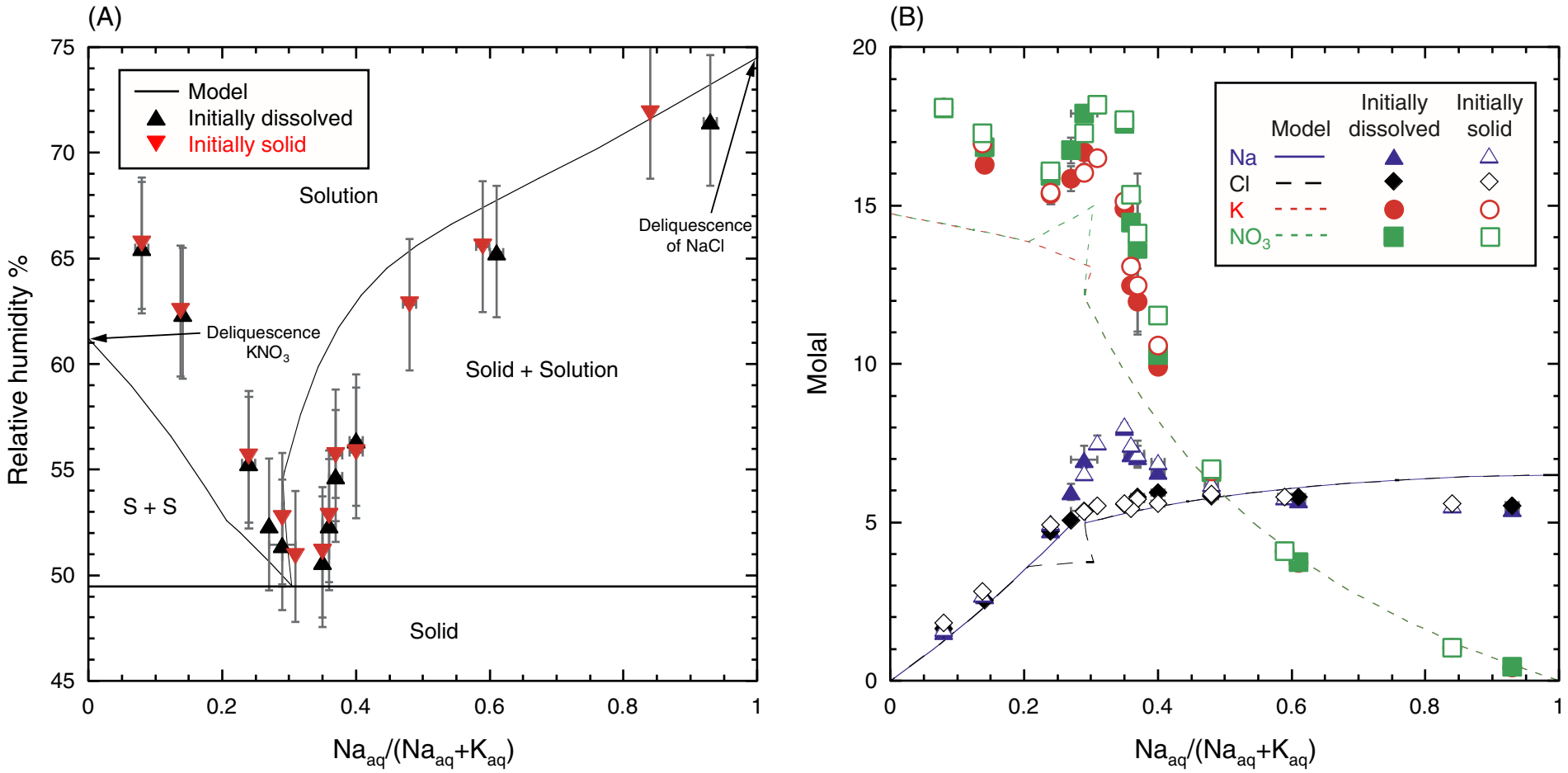

Figure 4. Deliquescence of $NaCl$-KNO_3 salts at 90ºC starting from initially dissolved and initially solid mixtures plotted as (A) % relative humidity and (B) solution composition.

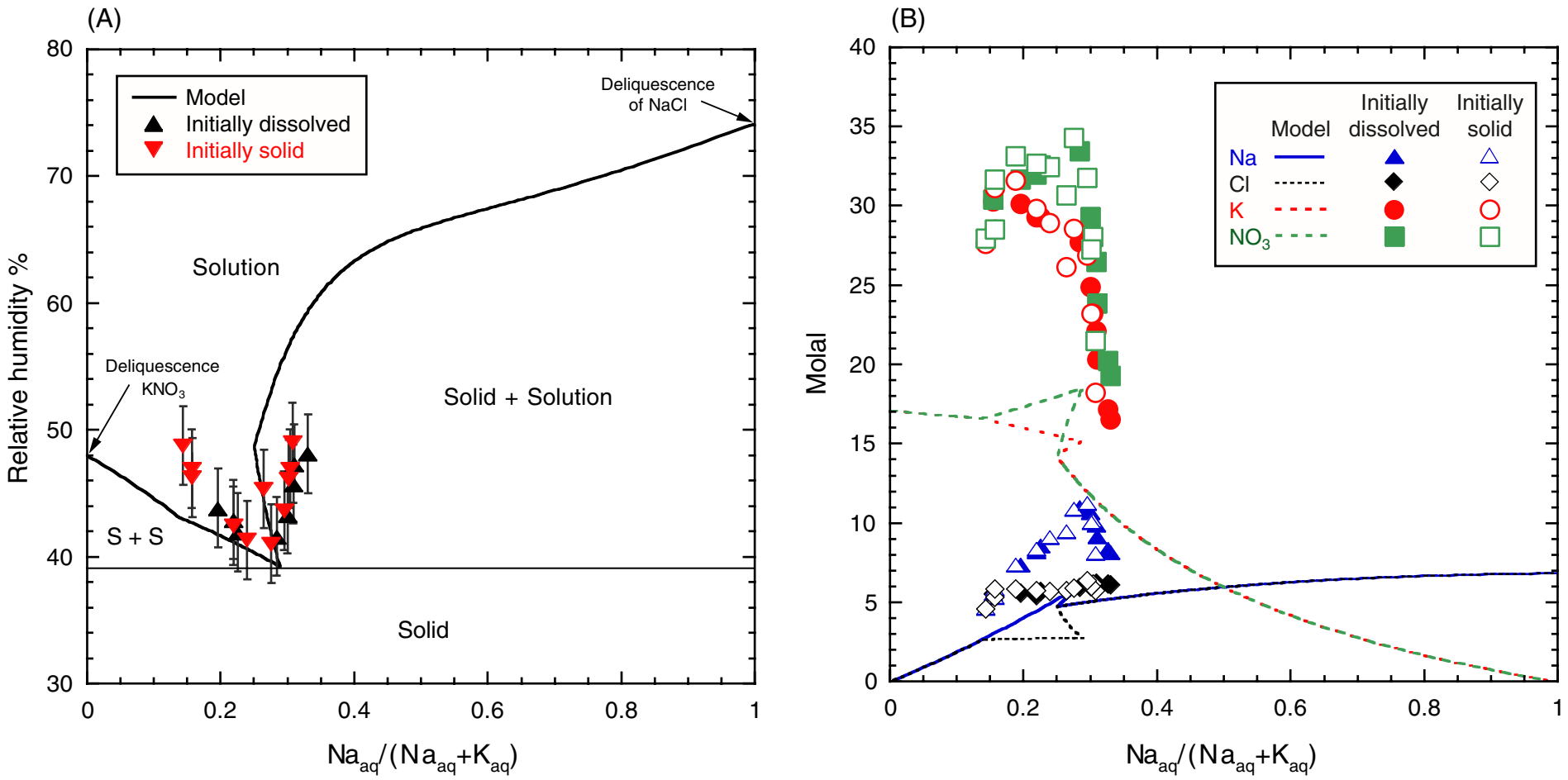

Figure 5. Deliquescence of NaCl-KNO_3 salts at 120ºC starting from initially dissolved and initially solid mixtures plotted as (A) % relative humidity and (B) solution composition.

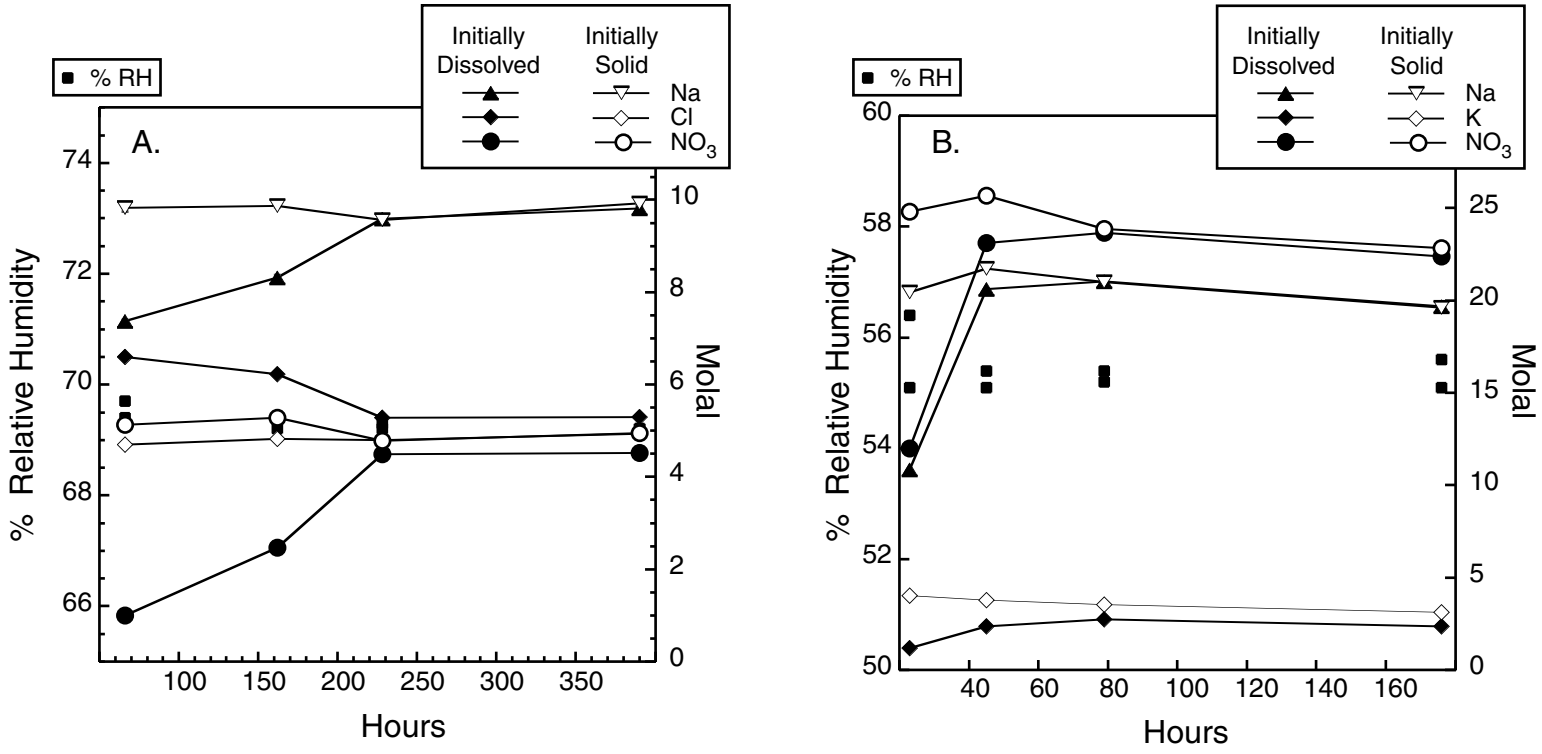

Figure 6. Examples of the brine % relative humidity and composition as a function of time for the reversed deliquescence experiments at 90ºC for (A) $NaCl$-$NaNO_3$ and the (B) KNO_3-$NaNO_3$ mixtures.

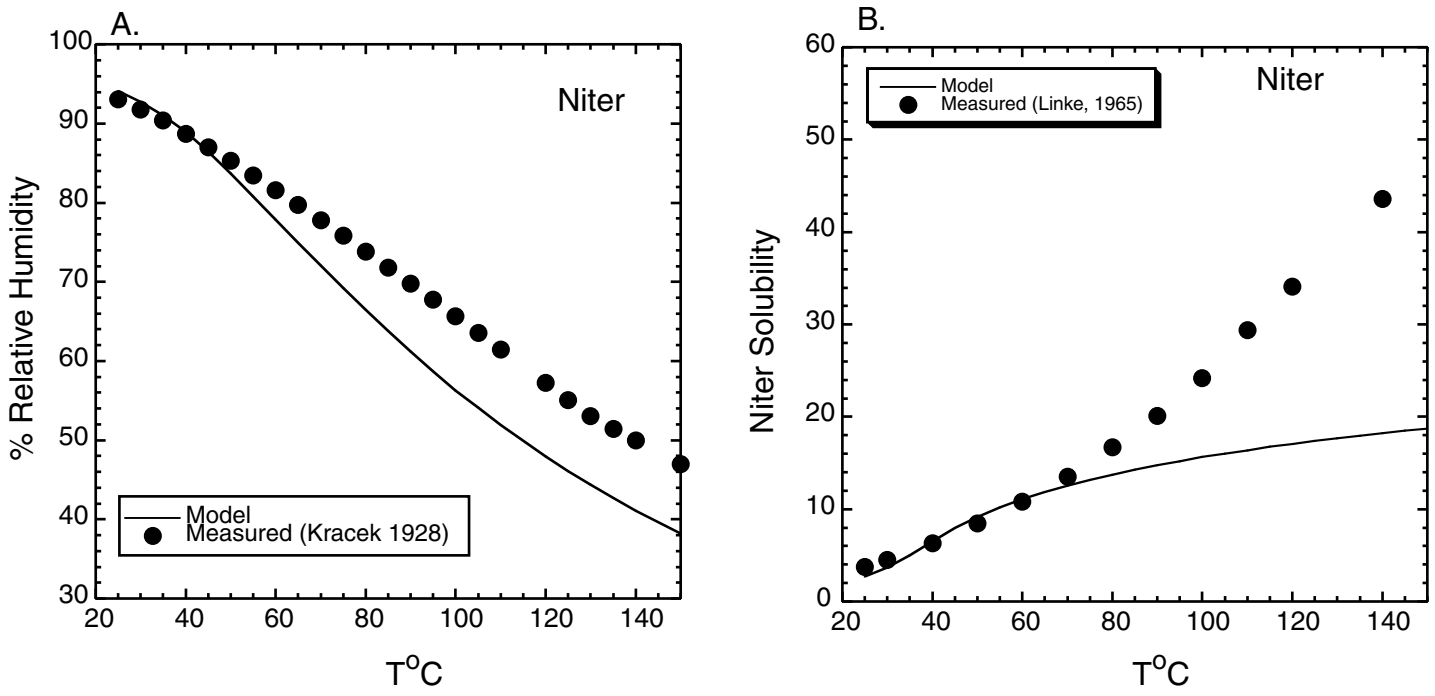

Figure 7. Comparison of predicted and measured niter (KNO_3) (A) % relative humidity and (B) solubility as a function of temperature. Predictions were made using EQ3/6 version 8 geochemical code and the Yucca Mountain high temperatured Pitzer ion interaction thermodynamic data base (BSC 2003a,b).

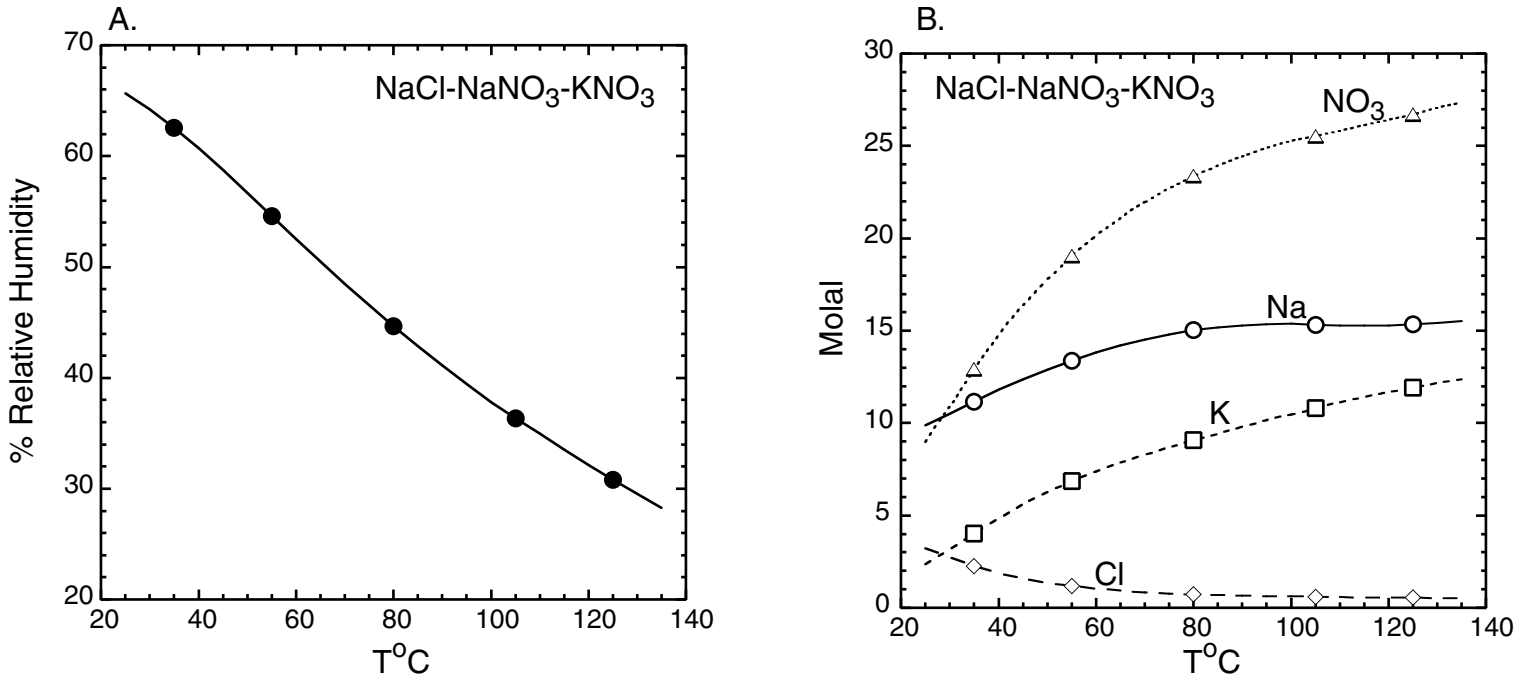

Figure 8. Model predictions of brine (A) % relative humidity and (B) solution composition as a function of temperature at the deliquescence point for a $NaCl$-$NaNO_3$-KNO_3 mineral assemblage (BSC 2003b). Predictions were made with EQ3/6 geochemical code and the high temperature Pitzer ion interaction thermodynamic data base. Triangles, circles, squares, and diamonds represent NO_3, Na, K, and Cl concentrations.